Brazilian Journal of Physics (2022) 52: 46
https://doi.org/10.1007/s13538-022-01057-z

GENERAL AND APPLIED PHYSICS

SQUID and Hall Effect Magnetometers for Detecting and Characterizing Nanoparticles Used in Biomedical Applications

Jefferson Ferraz Damasceno Felix Araújo[1] · Hélio Ricardo Carvalho[1,2] · Sonia Renaux Wanderley Louro[1] · Paulo Edmundo de Leers Costa Ribeiro[1] · Antonio Carlos Oliveira Bruno[1]

Received: 28 November 2021 / Accepted: 13 January 2022 / Published online: 29 January 2022

Abstract
We reviewed magnetometers built in our group to detect and characterize nanoparticles used in biomedical applications. The SQUID magnetometer was based on a custom-made bulk rf-SQUID and a magnetizing coil. We measure sample magnetic moments using a thermoremanent magnetization technique by applying a magnetic field while lowering the temperature of the nanoparticles below their blocking temperature. Commercial nanoparticles routinely used in magnetic immunoassays were tested. The limit of sensitivity of our SQUID system was estimated to be 10^{-14} A m^2. In addition, we built modular Hall effect magnetometers to characterize custom-made nanoparticles covered with a polymer able to function as a drug carrier. The influence of the coating in the magnetic core was studied. We acquired magnetization curves from room temperature down to 10 K. Zero-field cooling and field cooling curves were obtained as well. The magnetometers built were compared successfully to commercial stand-alone equipment. Finally, we presented a simple magnetometer developed to be used in a classroom laboratory in order to measure the saturation, remanence, and coercive fields of iron oxide microparticles.

Keywords Magnetometers · SQUIDs · Nanoparticles · Superparamagnetism

1 Introduction

There has been an increase in the use of magnetic nanoparticles in biomedical applications [1]. They can be covered with biocompatible materials that can be functionalized, transforming them into biosensors to search and capture viruses, bacteria, and other microorganisms [2]. In addition, they can be used to transport drugs, which can be delivered to the desired location inside the body; furthermore, they can be used to perform local hyperthermia and destroy tumor cells [3].

To be manipulated properly, nanoparticles must be superparamagnetic at room temperature [4]. A key feature of this property is the absence of coercivity and remanence. This property guarantees a low tendency for nanoparticles to agglomerate. As a necessary condition, its magnetic core, usually made of iron oxide, needs to be fabricated in sizes below 100 nm.

Due to the absence of commercial equipment in our university for detecting and measuring magnetic properties of materials, long ago we made a strategic decision to build our own magnetometers. Along the last decade, we developed a series of magnetometers based on several sensing technologies such as the Hall effect [5–13], magnetoresistive effect [14], magnetostriction effect [15, 16], magneto-optical effect [17], and superconducting quantum interference device (SQUID) [18–21]. In this review, we will address some magnetometers we built based on the Hall effect and SQUID devices [6, 7, 10, 21]. The Hall effect magnetometers were designed to characterize homemade iron oxide nanoparticles coated with a polymer. The magnetometer based on the SQUID was developed for detecting commercial nanoparticles used in magnetic immunoassays [22].

2 The Devices

There are countless Hall effect devices commercially available. Devices known as Hall effect elements consist of a four-terminal package which encapsulates a semiconductor

✉ A. C. Bruno
acobruno@gmail.com

[1] Departamento de Física, Pontifícia Universidade Católica do Rio de Janeiro, Rio de Janeiro, RJ 22451-900, Brazil

[2] Instituto Nacional de Metrologia, Qualidade e Tecnologia, Rio de Janeiro, RJ 25250-020, Brazil

of submillimeter size. One needs to apply a milliampere current to measure the Hall voltage that is proportional to the detected magnetic field. Devices known as Hall effect sensors are far more elaborate, consisting of semiconductor plates of about the same size, plus amplifiers, filters, and temperature-compensating circuits inside the same package. Some have a programmable gain and offset voltage. Usually, one needs to apply 5 V to bias the sensor. Each type has its own strengths and applications, as we shall see. Hall effect devices are extremely affordable; the elements cost less than $1 each, and sensors cost up to $5 each.

The SQUID magnetometer built was based on a bulk radio-frequency SQUID [23]. Long ago, we had built SQUID sensors with help of one of its inventors, James Zimmerman, during his visits to our laboratory [18]. The peculiarity about the constructed SQUIDs is the fact that its Josephson junction is made by using two Nb wires pressed against each other. This makes them virtually immune to effects of humidity and thermal shocks since the Josephson junction can be readjusted repeatedly if needed. An extra layer of protection against humidity can be made by oxidizing the Nb wire, heating it for few minutes at few hundred degrees. We have called it the wj-SQUID (wire-junction SQUID). Bulk SQUIDs have not the highest sensitivity among other SQUID designs; nevertheless, they have sufficient sensitivity for performing magnetic immunoassays.

We designed the wj-SQUID considering our sample holder, a 50 µL glass micropipette having a 1.45 mm outside diameter. The SQUID holes were made with a 1.5 mm diameter, just big enough to be filled with the micropipette. The length of the hole was set to 4.0 mm, so that its self-inductance was 0.25 nH, about the same self-inductance of the SQUIDs we built previously. The RF-coil was redesigned to bias the SQUID properly and to increase to 80 µV its characteristic triangular response. It has a diameter of 1.1 mm and 7 turns.

Bulk SQUIDs have higher inductance than thin-film SQUIDs. This fact leads to higher flux noise. However, they are cost effective and can be built from a 10 mm-diameter NbTi rod, with tools available at common machine shops. The 0.8 mm Nb wire used to make the Josephson junction can be bought online from several suppliers.

The lower limit for the detectable flux was set by applying 4.0 nA to the RF-coil and measuring the response. It was the lowest DC our current source (Keithley 6220, Tektronix Inc.) could supply. This current generates a magnetic moment of 2.4×10^{-14} A m^2 in the RF-coil. In response, the wj-SQUID generated an output of 1.8 mΦ_0, where Φ_0 (2.07×10^{-15} Wb) is the flux quantum.

In Fig. 1, schematic drawings of all devices that have been used to build the magnetometers are depicted. The drawings use the same scale: the Hall effect elements HQ-0811 (1) and HG-176A (2) from AKM Inc., the Hall effect sensor

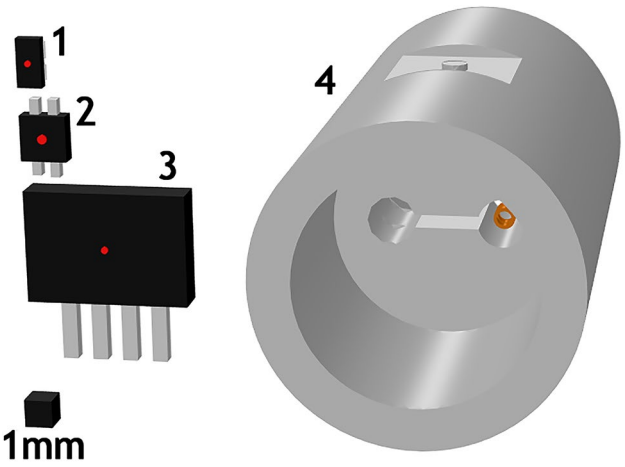

Fig. 1 Schematic drawing of Hall effect devices HQ-0811 (1), HG-176A (2), MLX90215 (3), and the homemade wj-SQUID (4). The red dot on the faceplate of the Hall effect devices shows the active sensing area. The wj-SQUID RF-coil is represented at its right-hand side hole

MLX90215 (3) from Melexis Inc., and the wj-SQUID (4). The red dot on the faceplate of the Hall effect devices represents the active sensing area. In the right-hand side hole of the wj-SQUID, the RF-coil is represented. Connected to a tank circuit, it provides the appropriate bias to the SQUID.

The magnetic noise spectrum of the Hall effect and SQUID magnetometers are displayed in Fig. 2 up to a frequency of 6.0 Hz. After biasing the MLX90215 with 5.0 V_{dc}, it was connected directly to the spectrum analyzer input (SR760, Stanford Research Inc.). This was possible due to its internal amplifier and filters. On the other hand, the

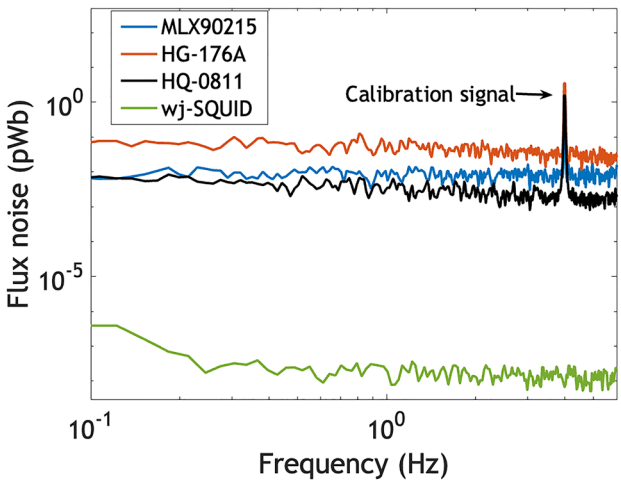

Fig. 2 System flux noise against frequency. Hall effect devices were calibrated with a 50 µT field at 4.0 Hz applied through a Helmholtz coil pair. Approximately 2 pWb in flux. The SQUID is calibrated in terms of the flux quantum Φ_0 (2.07×10^{-15} Wb)

Table 1 Hall effect and wj-SQUID magnetometer sensitivities. The devices' sensing areas are also reported

Devices	Sensitivity (mV/pWb)	White noise (fWb)	Area ($\times 10^{-8}$ m^2)
HG-176A	5.2	25	7.1
HQ-0811	15	2.0	3.1
MLX90215	2.8	10	4.0
wj-SQUID	80,000	0.0002	88

HG-176A and HQ-0811 were biased with an AC at 1.0 kHz with a 1.0 mA peak and a lock-in amplifier (SRS830, Stanford Research, Inc.) was used to provide appropriate gain and filtering. In order to calibrate the Hall effect devices, we used a Helmholtz coil pair generating a 4.0 Hz field with an RMS value of 50 μT, about the earth's magnetic field. The average flux through the area of the Hall effect devices was about 2 pWb. In order to bias, filter, and amplify the wj-SQUID signal, we used dedicated electronics (Control Unit 30, S.H.E. Corp.).

Regarding sensitivity, Hall effect devices are in the low end among magnetic sensing technologies when compared to SQUID devices. Table 1 reports the sensitivities in mV/pWb. Note the difference in orders of magnitude on the sensitivities between the Hall effect devices and the SQUID. The device HQ-0811, with an InAs element inside it, has a higher gain and about one order of magnitude less noise than the HG-176A which has a GaAs element. It must be emphasized that owing to its high sensitivity, the SQUID is usually operated inside a small magnetic shielded chamber.

3 The Model

To relate the measured magnetic field to sample magnetization, a mathematical model must be used. All commercial magnetometers model samples as a magnetic dipole. This can be done because the samples used can be made small and are placed at some distance from the sensors, so their shape can be neglected. In our case, just the opposite occurs, our samples are big in relation to the sensor size, and our sensors need to be placed very near the sample, so its shape must be considered.

For practical reasons, we chose to shape our nanoparticle samples in a cylindrical format. For the Hall effect magnetometers, we used a sample holder having a cylindrical cavity with a 3.1 mm diameter, 3.0 mm long. This size was chosen in order to fit a commercial Ni sphere used to calibrate the magnetometer. To fill completely this cavity, we need about 15 mg of nanoparticles. For the SQUID magnetometer, we used 50 μL glass micropipettes whose inside diameter was 0.85 mm. We filled them with typically few micrograms of the nanoparticle solution yielding about 2.0 mm in length.

Assuming the nanoparticles were evenly distributed inside the sample holder, we model the sample as a cylindrical current sheet with radius R and length L, having an equivalent bound current I_b as shown in Fig. 3. The bound current times the area of the cylinder provides the desired magnetic moment of the sample. Depending on the magnetometer used, the radial or longitudinal field component generated by the model was calculated. Since there is no closed analytical solution for the flux generated by the cylindrical current sheet through the sensors, a numerical approach was used.

4 wj-SQUID Magnetometer

Immunoassays aim to quantify the presence of antigens on a sample that could be plasma or blood from a patient. Magnetic nanoparticles can be functionalized with antibodies, allowing them to search and capture viruses, bacteria, and other microorganisms. Once linked to the nanoparticles, we can use the magnetic moment of the sample to quantify the amount of the captured antigens [22].

The measurement consists of introducing the micropipette containing the nanoparticles directly into the SQUID

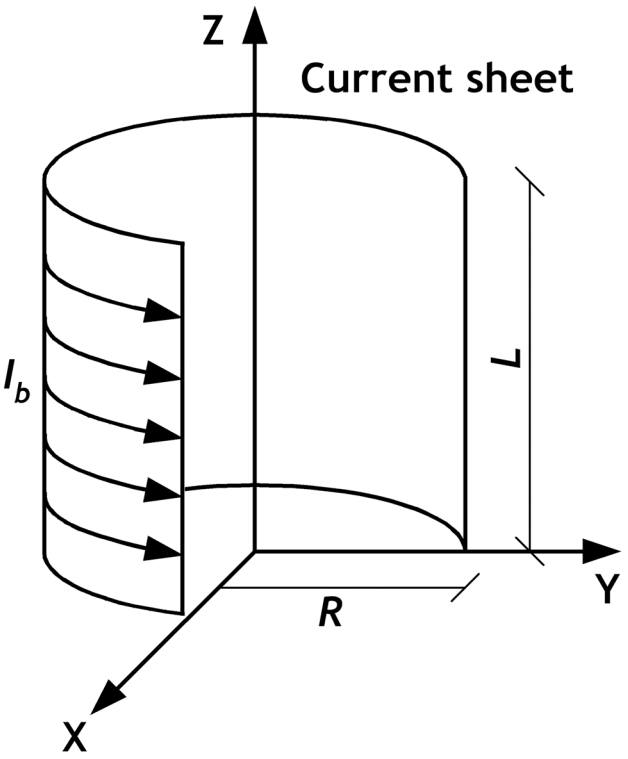

Fig. 3 Representation of the cylindrical current sheet model having a loop of radius R and length L and with equivalent bound current I_b

hole and of observing the change in flux. The nanoparticles are superparamagnetic at room temperature; thus, in order to create a remanent magnetic moment to be measured, a thermoremanent magnetization process was used [24]. By cooling the nanoparticles below their blocking temperature in the presence of a magnetic field, remanence appears. Establishing a measurement time window, the blocking temperature is defined as the temperature that switches the nanoparticles' moment relaxation from fast to slow. Measuring remanence at low temperatures enables us to quantify the sample magnetic moment.

The SQUID probe is shown schematically in Fig. 4. A stainless tube (4) holds a cylindrical magnetizing coil (2) and the SQUID (3) together. The coil generates 10 mT at its center for each ampere of current. The micropipette is also depicted in Fig. 4 housing the nanoparticles (1). The measurement procedure consists of positioning the nanoparticles at the center of the magnetizing coil with the SQUID and coil inside the liquid helium container but outside the helium bath. We turned on the current in the magnetizing coil while the SQUID probe is lowered into the helium bath. This procedure takes less than 30 min. When inside the bath, we turn off the coil current and turn on the SQUID electronics. Next, the micropipette is inserted in the SQUID hole. The SQUID outputs can be seen in Fig. 5 for different nanoparticles and various applied fields. For each new sample, this procedure is repeated. We used nanoparticles Nanomag-D-spio [25] which are coated with dextran, with a 50 nm average hydrodynamic diameter. We used also Estapor M1-020/50 [26], coated with polystyrene, with a 176 nm average hydrodynamic diameter. Both particles are commercially available to perform magnetic immunoassays.

We prepared the Nanomag sample from 5.0 µL of the original solution that contains 50 µg of particles with 35% of magnetite in weight. The Estapor sample was also prepared from 5.0 µL of the original solution that contains 250 µg of particles with 52% of ferrite in weight. We mixed the nanoparticles with an epoxy resin. A mass of 1.4 µg of the Nanomag mixture was placed inside the micropipette. The Estapor mix, having a mass of 16 µg, was introduced into another micropipette. We demagnetized (Realistic Bulk Tape Eraser 44-232) both mixtures and remagnetized them with a series of magnetic fields during the thermoremanent process.

The SQUID flux as a function of the position of the center of the mixture is displayed in Fig. 5. The origin was taken as the center of the SQUID hole. We applied, at the sample containing 16 µg of Estapor, 0.5 mT (dashed line) and 2.5 mT (solid line). The latter generated a flux inside the SQUID of 4.9 pWb. We changed the sample to 1.4 µg of Nanomag and increased the applied field to 5 mT (dotted line) and to 10 mT (dash-dotted line). The flux generated was 0.5 pWb and 0.8 pWb, respectively. It was observed that the relation between the SQUID flux and the applied field was not linear. It should be noted also that the applied fields were far from the fields needed to saturate both samples.

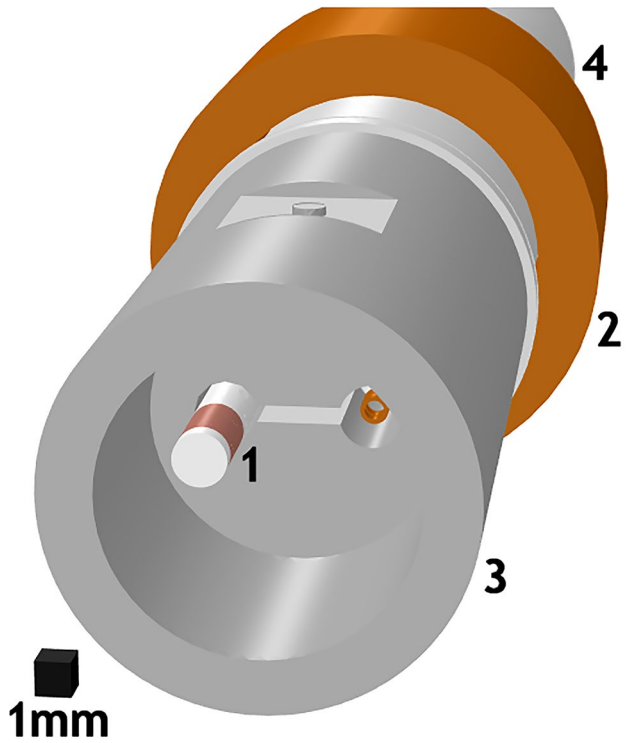

Fig. 4 Schematic drawing of our SQUID magnetometer probe with the glass micropipette having the tip filled with nanoparticles (1), magnetizing coil (2), wj-SQUID (3), and stainless steel tube that holds the SQUID and coil together (4)

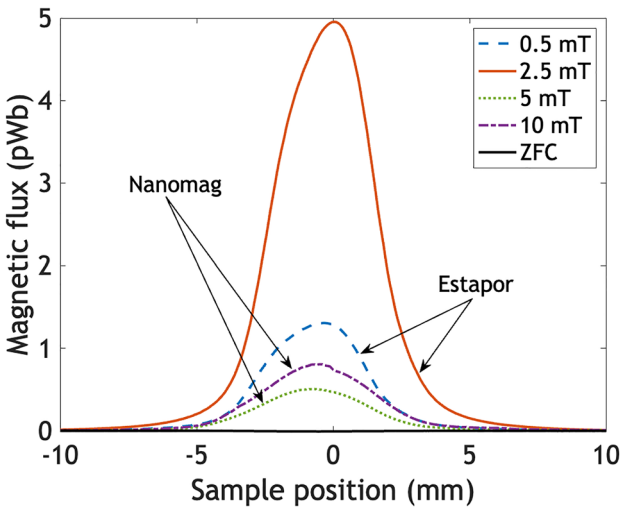

Fig. 5 Magnetic flux as a function of sample position relative to the center of the SQUID hole, due to the process of thermoremanent magnetization of Nanomag-D-spio and Estapor M1-020/50. Different colors indicate different applied fields. ZFC means zero-field cooling

Using the cylindrical current sheet model, the maximum remanent magnetizations obtained for the Estapor and Nanomag samples were 1.9 A m^2/kg and 3.8 A m^2/kg, respectively. The minimum detectable mass for Estapor and Nanomag particles can be estimated, using 1.8 mΦ_0 as the smaller flux detected by the wj-SQUID. This led to a minimum detectable mass of 12 pg and 4.0 pg, respectively.

5 Hall Effect Magnetometers

5.1 Room-temperature Magnetometer

We built a magnetometer, for room-temperature nanoparticle characterization, consisting of a set of four MLX-90215 linear programmable Hall effect sensors. The sample holder (1), electromagnetic pole (2), sensors (3), and supporting structure (4) can be seen schematically in Fig. 6. The structure was made of transparent acrylic. The sample holder has a cuboid shape with a cylindrical cavity with a 3.1 mm diameter, 3.0 mm long at its bottom filled with nanoparticles. It is straightforward to assemble the magnetometer; just attach the structure to one of the electromagnetic poles with a double-sided adhesive tape. The two sensors at the vertical position, aligned with the electromagnetic pole face, measure the applied field. To maximize the applied field dynamic range, we programmed one sensor for positive and the other for negative fields. The sensors placed on the horizontal are in a planar gradiometric configuration. The one on the left-hand side senses only the field generated by the poles, since neither can be positioned exactly perpendicular to the pole face. This signal is subtracted from the sensor on the right-hand side placed just below the sample. The sensors were connected directly to a data acquisition board (USB-6210, National Instruments Inc.). We used an electromagnet (3470 GMW, Inc.) with 40 mm-diameter poles that generates a 1.0 T field with a 6 mm pole gap with a 3.0 A current. A complete magnetization curve is acquired in about 5 min. A thermocouple glued to the pole near the sensors detected no change in temperature for an entire sweep from 1.0 to −1.0 T and back to 1.0 T.

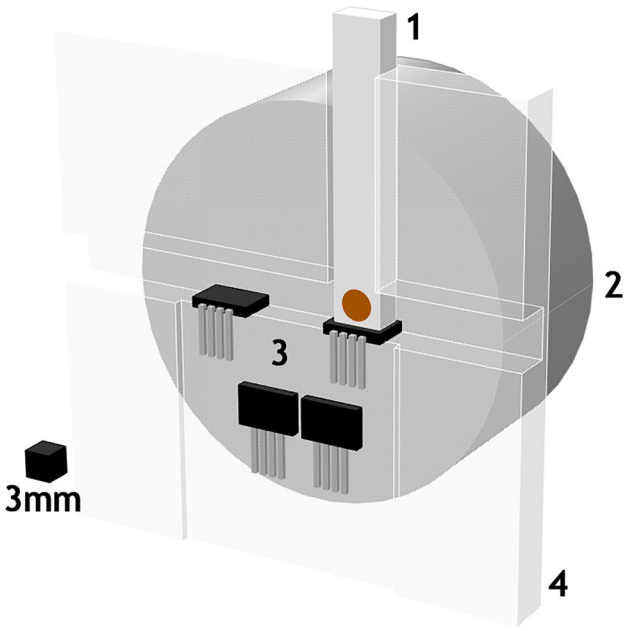

Fig. 6 Schematic drawing of the room-temperature magnetometer. The sample holder (1) filled with iron oxide particles is shown pressed against one of the sensors. The electromagnetic pole (2), four MLX90215 Hall effect sensors (3), and the acrylic support (4)

To obtain an accurate magnetic moment of the sample from the field generated by it, a calibration procedure must be executed. Since the sample magnetic field depends on the sensor-to-sample distance, this distance must be known as accurately as possible. The calibration procedure consists of measuring the magnetic field of a Ni sphere, whose magnetization is known, and of using the magnetic dipole model to find the sensor-to-sample distance. We used as a reference the NIST magnetization standard of 54.94 ± 0.16 A m^2/kg at 0.5 T for a 99.99% pure Ni sphere [27]. We performed successfully the calibration using a 99% pure Ni sphere (Goodfellow, Inc.) with a 3.0 mm diameter weighing 126 mg. After several measurements, the average fitting result obtained for the sensor-to-sample distance was $x = 1.63$ mm, $y = 0.10$ mm, and $z = 2.30$ mm. To validate the result, we used this distance, the measured Ni magnetic field, and the dipole model to find 54.66 ± 0.27 A m^2/kg at 0.5 T, half percent different from the NIST standard. Our result is displayed in Fig. 7 (solid line). We compared our measurements to a commercial MPMS SQUID system (Quantum Design, Inc.) using the same Ni sphere (dashed line). The result at 0.5 T was 54.92 A m^2/kg. It is also displayed in Fig. 7 the NIST magnetization standard (square). Using a signal-to-noise ratio of 1:1 criterion, we estimated 3.5×10^{-7} A m^2 as the magnet moment sensitivity of this magnetometer.

Our intent was to fabricate our own nanoparticles and study its functionalization. Functionalization involves the coating of the magnetic core with different materials in several layers. This will modify the distance between the nuclei, affecting the magnetic inter-particle interactions. We were particularly interested in studying the triblock copolymer Pluronic F-127 (BASF SE) as nanoparticle coating that would be able to work as a drug carrier.

Therefore, we used the coprecipitation method to fabricate the iron oxide nuclei [6, 7]. The method is straightforward and produces a wide range of magnetic nanoparticles, presenting several benefits, such as low cost, rapid reaction time, large quantities, and nanoparticles with few agglomerations. The nanoparticles average size and distribution can

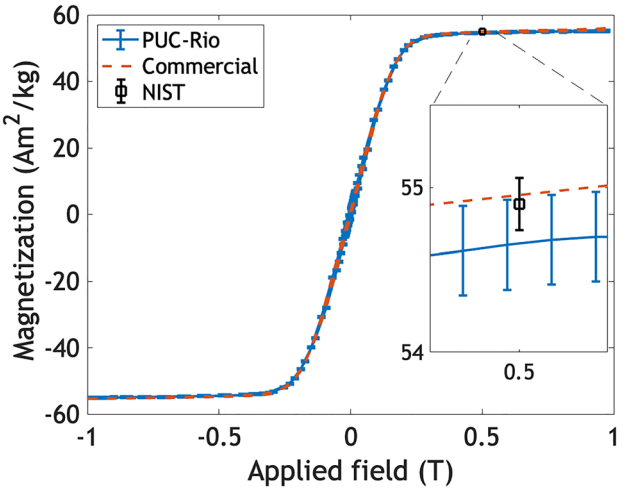

Fig. 7 Magnetization curve of a Ni sphere obtained after our calibration routine (solid line). The error bar is ± 0.27 A m^2/kg. Same sphere measured on a commercial MPMS SQUID from Quantum Design Inc. (dashed line). The NIST magnetization standard for 99.99% pure Ni is 54.94 ± 0.16 A m^2/kg at 0.5 T (square)

be controlled by changing parameters such as ionic strength and pH. We characterized the obtained iron oxide nanoparticles by transmission electron microscopy and X-ray diffraction, revealing peaks representative of magnetite with an average size of 9 nm [7]. In Fig. 8, the magnetization obtained as a function of the applied field is displayed. The magnetization of the uncoated particles (solid line) does not show relevant hysteresis effect as desired. Then, Pluronic F-127 was added in percentages of the total mass of 10%

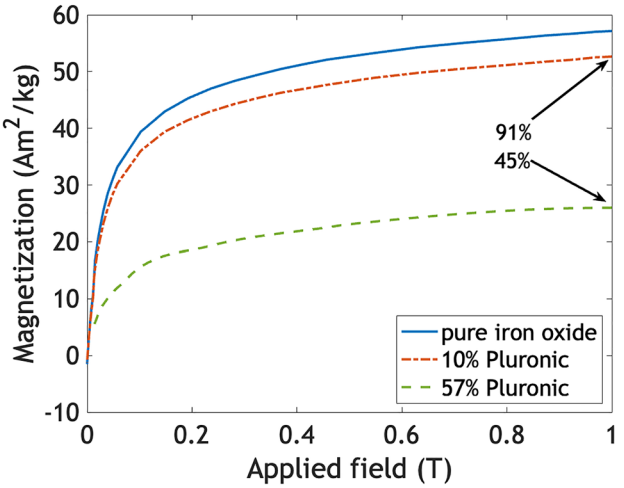

Fig. 8 Magnetization curves for different coatings percentages as a function of the applied field. The amount of Pluronic F-127 in percentage of the total mass is 0% (solid), 10% (dash-dotted), and 57% (dashed). We observed a reduction to 91% and 45% of the magnetization, respectively, in relation to the pure iron oxide magnetization

(dash-dotted line) and 57% (dashed line). It can be noticed that the magnetization curves of the coated particles have the same outline and the values at saturation are reduced to 91% and 45%, respectively, in relation to the magnetization of the uncoated particles. This was an indication that the magnetic moments of the particles were independent of the coating [7].

5.2 Classroom Magnetometer

A simpler version of the room-temperature magnetometer was built to be used by students in an electricity and magnetism classroom laboratory. Figure 9 shows a schematic drawing of the setup: the sample holder (1), the NdFeB magnet block (2), two MLX90215 Hall effect sensors (3), and the transparent acrylic support (4). The replacement of the electromagnet by two 40 × 20 × 10 mm blocks of NdFeB N42 grade magnets reduces the maximum applied field down to 0.4 T, which is, nevertheless, enough to drive

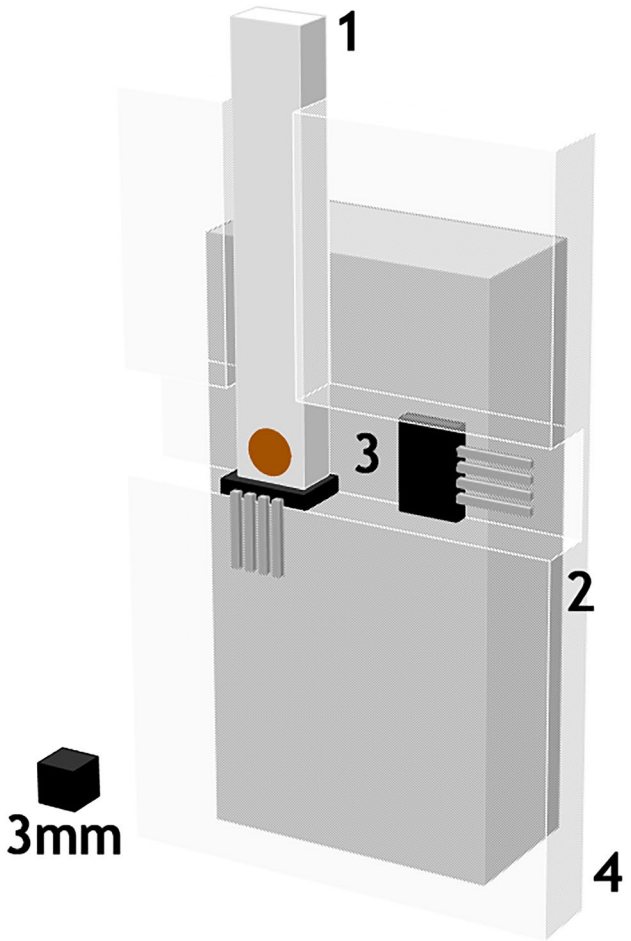

Fig. 9 Schematic drawing of the classroom magnetometer: sample holder (1), NdFeB magnet (2), two MLX90215 Hall effect sensors (3), and acrylic support (4)

the sample made of iron oxide microparticles (RW-222, Metal-Chek do Brasil, Ltda.) to magnetic saturation.

There is also an aluminum track (not shown) in which the magnets are displaced. Three experiments were proposed: (i) assembling the magnetometer itself; (ii) measuring the saturation and remanent and coercive fields of the iron oxide sample; and (iii) using a magnetic dipole model to obtain the approximate magnetization values. The sensors were connected directly to a digital multimeter. The field values for the sample response can be obtained by dividing the output voltage by the sensor-programmed gain. In the case of the sensor detecting the sample, the value was 60 mV/mT, and in the case of the sensor detecting the field due to the magnet, 3 mV/mT. To obtain the magnetization curve, we start the measurements by displacing the magnets in the track from a position near the sample (high field) to a position far away from it (low field). Then, we remove the sample and measure again, displacing the magnets back to the starting position. We need two sets of measurements because the sensor near the sample detects also a stray field from the magnets. The difference between the two sets gives us just the contribution of the sample. Figure 10 shows the sample magnetization values. In order to obtain the coercive field, we moved the magnets to the end of the track and turned them by 180°. The dashed lines indicate the values obtained for saturation, remanence, and the coercive field, 3.5 mT, 0.4 mT, and − 8.0 mT, respectively. We estimated the magnet moment sensitivity of this magnetometer to be 2.5×10^{-5} A m^2, using a signal-to-noise ratio of 1:1 criterion.

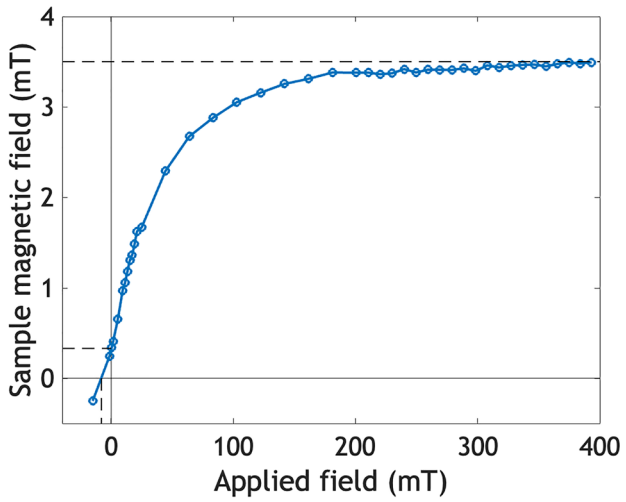

Fig. 10 Measurements of the classroom magnetometer. The dashed lines mark the saturation and remanent and coercive fields

5.3 Low-temperature Magnetometer

We were additionally interested to study the magnetic behavior of nanoparticles at low temperatures. We faced the challenge to fit a magnetometer in a 12 mm-diameter cylindrical chamber, 5 cm long inside a closed-cycle cryocooler (DE-202AF, ARS Inc.). We had to change from the Hall effect sensors used before to a single much smaller Hall element.

A schematic drawing of the low-temperature magnetometer can be seen in Fig. 11. It displays the sample holder (1), Hall element (3), and linear track (4) all inside the cryocooler tail (5). One electromagnetic pole (2) is also represented. The linear track and sample holder were built using a machinable glass ceramic material (MACOR, Corning Inc.) that has a low coefficient of thermal expansion.

The sample holder slides up and down in the linear track over the Hall effect element. It is set in motion by a micro-linear actuator (X-NA08A50, Zaber Inc.). The scan starts when the signal is maximum, with the sample on top of the Hall effect element, and finishes when the signal reaches a minimum at about 25 mm far away from it. This process is repeated for a series of values of applied field.

Datasheets for non-cryogenic Hall elements specify the minimum operating temperature as −40 °C. However, the ones we tested made of GaAs worked well down to 6 K. Between the ones we have tested, the HG-176A presented

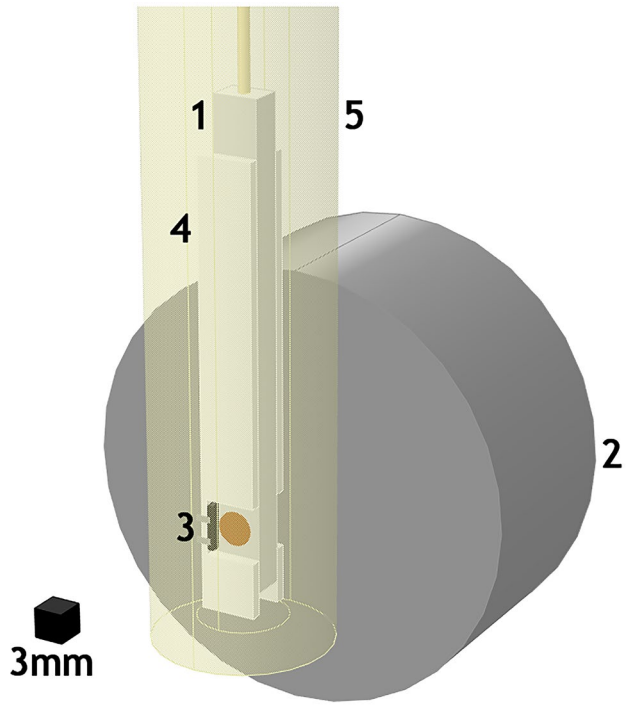

Fig. 11 Magnetometer showing a schematic drawing of sample holder (1), 40 mm-diameter electromagnetic pole (2), HG-176A Hall effect element (3), linear track (4), and cryocooler tail (5)

the best performance regarding linearity and reliability. It incorporates a GaAs sensing element with a 300-μm diameter, with a distance of 200 μm from the top surface. For measurements down to 100 K, a better choice is the InAs Hall effect element HQ-0811, which has higher gain and noise levels one order of magnitude lower than those of the HG-176A.

Using a four-wire resistance method, we measured the bare sensitivity of the HG-176A at different temperatures as depicted in the inset of Fig. 12. The response presented consistent linear measurements after several temperature cycles between 298 and 10 K. However, as can be seen in Fig. 12, the device sensitivity increased nonlinearly from 2.1 mV/mT at room temperature up to 2.6 mV/mT at 10 K. In order to provide accurate operation at each temperature, the new sensitivity was determined, preceding each measurement, by means of a coil attached to the outside of the cryocooler tail, generating a small magnetic field. The fact that the HG-176A presented a linear response for a broad temperature range was a key factor to the magnetometer design, allowing the sensor and sample to be at the same temperature chamber.

In its simplest configuration, the Hall effect element can be biased with DC, and the Hall voltage measured just by using a simple multimeter in a four-wire resistance mode. However, we obtained a much better signal-to-noise ratio using an AC bias and a lock-in amplifier to measure the Hall voltage. We attained an overall magnetic moment sensitivity of 8.5×10^{-8} A m^2 using a 1:1 signal-to-noise ratio criterion.

As far as the low-temperature magnetometer calibration is concerned, we have increased the calibration accuracy, by using two 99% pure Ni spheres separated by a specific distance. The magnetization results obtained at saturation against temperature can be observed in the first and second columns of Table 2. The third and fourth columns are for comparison with the values obtained for pure Ni by Crangle and Goodman [28]. The maximum absolute difference between the two sets of measurements was ± 0.2 A m^2, which is less than half percent. Note that the magnetization difference could be attributed to the slight difference in the temperature sets.

Table 2 Magnetization of Ni at saturation for low temperatures, obtained after our calibration process. The third and fourth columns are from Crangle and Goodman [28]

T (K)	M (A m^2/kg)	T (K)	M (A m^2/kg) [28]
241	56.4	239.8	56.38
174	57.2	176.7	57.39
144	57.8	138.8	57.82
114	58.1	113.6	58.06
76.3	58.5	75.7	58.30
21.8	58.6	25.2	58.52
11.6	58.6	12.6	58.56

Besides traditional magnetization curves, zero-field cooling and field cooling (ZFC-FC) curves can also be obtained. An example can be seen in Fig. 13 for our homemade iron oxide nanoparticles. ZFC curves are obtained cooling the sample without any applied magnetic field down to the desired temperature, and then magnetization was measured heating the sample and applying a small field, in this example 9 mT (squares). FC curves are obtained by cooling the sample at the same applied field until the desired temperature is reached (circles). From these curves for instance, the blocking temperature and average nanoparticle size can

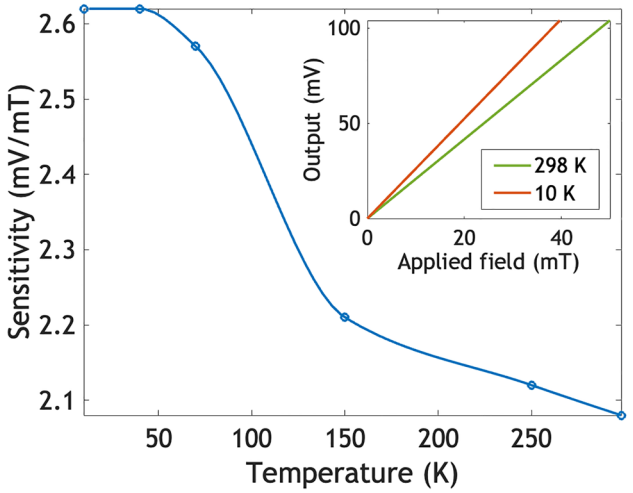

Fig. 12 Sensitivity of the Hall effect element HG-176A for operation at different temperatures. The inset shows a linear response from room temperature down to 10 K

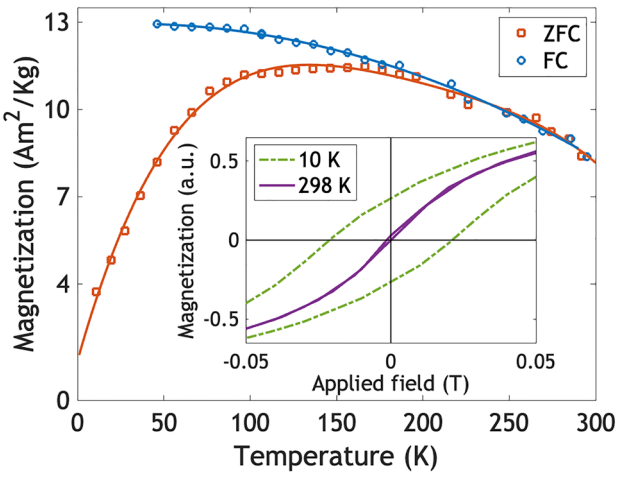

Fig. 13 ZFC-FC curves for pure iron oxide nanoparticles. The applied field was 9 mT. The inset shows the change in the magnetization curves from room temperature to 10 K

Table 3 Magnetometer type, magnetic moment sensitivity, and sample mass requirement

Magnetometer	Sensitivity (A m^2)	Sample mass (mg)
Room temperature	3.5×10^{-7}	15
Educational	2.5×10^{-5}	15
Low temperature	8.5×10^{-8}	15
wj-SQUID	2.4×10^{-14}	0.001

be obtained. The inset in Fig. 13 shows a detail (−0.05 to 0.05 T) of the normalized magnetization curve, when the temperature is changed from 298 K (solid line) to 10 K (dash-dotted line). Notice that at low temperature, remanence and coercivity become evident. These results agree with the theory for magnetic nanoparticles that predicts a magnetic phase change, from superparamagnetic to ferromagnetic, when measurements are made below the blocking temperature.

6 Concluding Remarks

We presented in this review the magnetometers built in our group with magnetic moment sensitivities ranging from 10^{-14} to 10^{-7} A m^2, allowing us to measure samples with masses ranging from micrograms to milligrams. We could also study samples in a wide range of temperatures, from room temperature down to 10 K. This allowed us to develop, in a timely manner, our own nanoparticles studying both the core and coating. In addition, we showed that magnetometers could be made simple enough to be used by students in a laboratory classroom. It was possible to measure the saturation, remanence, and coercivity of magnetic microparticles, properties approached only theoretically in undergraduate courses. Table 3 summarizes the sensitivities and the amount of mass of nanoparticles required for each magnetometer reported in this review.

Several other magnetometers were built by our group and not reviewed here [8, 9, 11, 12, 29–32]. It is worth mentioning the development of a class of magnetometers known as scanning magnetic microscopes, which we are successfully applying as well in other areas such as rock magnetism and to study industrial steels.

Acknowledgements We dedicate this contribution with great warmth to Prof. Sergio Mascarenhas, who, along several decades, provided constant incentive and wholehearted support to the activities of the Applied Physics Group at the Department of Physics at PUC-Rio. I (A.C. Bruno) had the privilege to be born in the family of Sergio, and since my early adolescence, I remember visiting him in São Carlos discussing my future. He accompanied me closely with great care and affection, from my scientific initiation to my postdocs, during my entire career and subsequent retirement. We never ceased to talk about the future, what to do next. I must say that most of the time I was amazed listening to his never-ending torrent of creative ideas. We would like to thank J.M.B. Pereira and M.C. Costa, participants in the original papers reviewed, and F. Osorio for helping with the noise measurements.

Funding This work was supported in part by the Brazilian agencies Conselho Nacional de Desenvolvimento Científico e Tecnológico (CNPQ), Coordenação de Aperfeiçoamento de Pessoal de Nível Superior (CAPES), and Fundação de Amparo à Pesquisa do Rio de Janeiro (FAPERJ).

Declarations

Conflict of Interest The authors declare no competing interests.

References

1. D.D. Stueber, J. Villanova, I. Aponte, Z. Xiao, V.L. Colvin, Pharmaceutics **13**, 943 (2021)
2. S. Liu, B. Yu, S. Wang, Y. Shen, H. Cong, Adv. Colloid Interface Sci. **281**, 102165 (2020)
3. C. Janko, T. Ratschker, T. Nguyen, N. Khanh, L. Zschiesche, R. Tietze, S. Lyer, C. Alexiou, Front. Onc. **9**, 59 (2019)
4. D.-L. Joanna, A. Łazarczyk, P. Hałubiec, O. Szafrański, K. Karnas, A. Karewicz, Materials **12**, 617 (2019)
5. J.F.D.F. Araujo, A.C. Bruno, H.R. Carvalho, J. Magn. Magn. Mater. **322**, 2806 (2010)
6. J.F.D.F. Araujo, A.C. Bruno, S.R.W. Louro, Rev. Sci. Instrum. **85**, 105103 (2015)
7. J.F.D.F. Araujo, M.C. Costa, S.R.W. Louro, A.C. Bruno, J. Magn. Magn. Mater. **426**, 159 (2017)
8. J.M.B. Pereira, C.J. Pacheco, M.P. Arenas, J.F.D.F. Araujo, G.R. Pereira, A.C. Bruno, J. Magn. Magn. Mater. **442**, 311 (2017)
9. J.F.D.F. Araujo, D.R.P. Vieira, F. Osorio, W.E. Pöttker, F.A. Porta, P. Presa, G. Perez and A.C. Bruno, J. Magn. Magn. Mater. **489**, 165431 (2019)
10. J.F.D.F. Araujo, J.M.B. Pereira, A.C. Bruno, Am. J. Phys. **87**, 471 (2019)
11. J.F.D.F. Araujo, A.L.A. Reis, A.A.P. Correa et al., Materials **12**, 4154 (2019)
12. J.F.D.F. Araujo, A. Soudabeh, F.L. Freire Jr. et al., J. Magn. Magn. Mater. **499**, 166300 (2020)
13. E.B.M. Junior, F.G. Osorio, F.V. Gutierrez et al., Measurement **171**, 108808 (2021)
14. E.A. Lima, A.C. Bruno, H.R. Carvalho, B.P. Weiss, Meas. Sci. Technol. **25**, 105401 (2014)
15. C.J. Pacheco, A.C. Bruno Meas. Sci. Technol. **21**, 065205 (2010)
16. S.M.M. Quintero, A.M.B. Braga, H.I. Weber, A.C. Bruno, J.F.D.F. Araújo, Sensors **10**, 8119 (2010)
17. C.J. Pacheco, A.C. Bruno, Sensors **13**, 11476 (2013)
18. A. C. Bruno, J. E. Zimmerman, in Superconducting Devices and Their Application, (Springer-Verlag, 1992) pp. 240–242
19. H. R. Carvalho, A. C. Bruno, S. R. W. Louro, P. Costa Ribeiro, IEEE Trans. Appl. Supercon. **17**, 820 (2007)
20. H. R. Carvalho, A. C. Bruno, S. R. W. Louro, P. Costa Ribeiro, IEEE Trans. Magn. **44** 4472 (2008)
21. H.R. Carvalho, A.C. Bruno, IEEE Trans. on Appl. Supercon. **21**, 481 (2011)
22. S. Wissberg, M. Ronen, Z. Oren et al., Sci Rep **10**, 1573 (2020)
23. J.E. Zimmerman, P. Thiene, J.T. Harding, J. Appl. Phys. **41**, 1572 (1970)
24. L. Neel, Rev. Mod. Phys. **25**, 293 (1953)

25. Micromod Partikeltechnologie GmbH, Friedrich-Barnewitz-Str.4, 18119, Rostock-Warnemuende, Germany
26. Merck KGaA, Frankfurter Str. 250, D-64293 Darmstadt, Germany.
27. Standard Reference Material 772a, NIST Gaithersburg, MD 20899, Certificate Issue Date: 10 June 2005
28. J. Crangle, G.M. Goodman, Proc. R. Soc. Lond., A Math. Phys. Sci. **321**, 477 (1971)
29. J.F.D.F. Araujo, A.L.A. Reis, V. Oliveira et al., Sensors **19**, 1636 (2019)
30. J.F.D.F. Araujo, F. Gutierrez, E. Yokoyama, G. Perez, G. Solorzano, Microsc. Microanal. **26**, 2762 (2020)
31. J. Moura, R. Loreto, J.F.D.F. Araujo, G. Solorzano, Microsc. Microanal. **27**, 3312 (2021)
32. F. Gutierrez, A. Falco, E. Yokoyama et al., Nanomaterials **11**, 2197 (2021)